

# Flavoring the production of Higgs pairs

M. A. Arroyo-Ureña,<sup>1,2,\*</sup> J. Lorenzo Díaz-Cruz,<sup>1,2,†</sup> E. A. Herrera-Chacón,<sup>3,‡</sup> T. A. Valencia-Pérez,<sup>4,§</sup> and J. Mejia Guisao.<sup>5,2,¶</sup>

<sup>1</sup>*Facultad de Ciencias Físico-Matemáticas,*

*Benemérita Universidad Autónoma de Puebla, C.P. 72570, Puebla, México,*

<sup>2</sup>*Centro Interdisciplinario de Investigación y Enseñanza de la Ciencia (CIIEC),*

*Benemérita Universidad Autónoma de Puebla, C.P. 72570, Puebla, México.*

<sup>3</sup>*Institute for Particle Physics Phenomenology,*

*Durham University, South Road, Durham, DH1 3LE*

<sup>4</sup>*Instituto de Física, Universidad Nacional Autónoma de México, C.P. 01000, CDMX, México.*

<sup>5</sup>*Departamento de Física, Centro de Investigación y de Estudios Avanzados del IPN,*

## Abstract

We present a study on the possibility of observing a hypothetical particle known as the Flavon  $H_F$ , which is predicted in an extension of the standard model that includes the so-called Froggatt-Nielsen mechanism. The proposed decay channel is through a  $b\bar{b}h$  final state, where the Higgs boson ( $h$ ) decays to a pair of photons or a pair of  $b$  quarks ( $h \rightarrow \gamma\gamma, b\bar{b}$ ). We found that, under special scenarios of the model parameter space, the processes analyzed could provide evidence for the existence of the Flavon in the next stage of the LHC: the High Luminosity LHC. Specifically, we predict a *signal significance* of  $5\sigma$  ( $2\sigma$ ) in the  $h \rightarrow b\bar{b}$  ( $h \rightarrow \gamma\gamma$ ) channel for a Flavon mass of 800 (900) GeV and an integrated luminosity of 2500 (3000)  $\text{fb}^{-1}$ .

---

\* [marco.arroyo@cfm.buap.mx](mailto:marco.arroyo@cfm.buap.mx)

† [jldiaz@cfm.buap.mx](mailto:jldiaz@cfm.buap.mx)

‡ [edwin.a.herrera-chacon@durham.ac.uk](mailto:edwin.a.herrera-chacon@durham.ac.uk)

§ [tvalencia@fisica.unam.mx](mailto:tvalencia@fisica.unam.mx)

¶ [jhovanny.andres.mejia.guisao@cern.ch](mailto:jhovanny.andres.mejia.guisao@cern.ch)

## I. INTRODUCTION

After the discovery of the Higgs boson by the ATLAS and CMS collaborations [1, 2] at the Large Hadron Collider (LHC), the particle physics community has focused on understanding the interactions of the Higgs boson with other particles, including itself. In the last years, the ATLAS and CMS collaborations have reported results on searches for di-Higgs proton-proton ( $pp$ ) production in the channels  $pp \rightarrow hh$ ,  $(h \rightarrow b\bar{b}, h \rightarrow b\bar{b})$ ,  $(h \rightarrow b\bar{b}, h \rightarrow \gamma\gamma)$ ,  $(h \rightarrow b\bar{b}, h \rightarrow WW^*)$ ,  $(h \rightarrow b\bar{b}, h \rightarrow ZZ^*)$ ,  $(h \rightarrow b\bar{b}, h \rightarrow \tau^-\tau^+)$  [3–7]. These searches have studied the different ways in which the Higgs boson is produced, such as  $ggh$ , VBF, in association with top-quark pairs, etc. We notice that in all channels the  $b\bar{b}$  pair prevails, motivated by these final states we undertake an analysis of production and decay of a scalar (so-called Flavon, denoted by  $H_F$ ) predicted in a model that implements the Froggatt-Nielsen (FN) mechanism [8], which we will refer to as the FN Singlet Model (FNSM). Such a model assumes that above some scale  $\Lambda$ , there is a symmetry (perhaps of Abelian type  $U(1)_F$ ) that forbids the appearance of Yukawa couplings; SM fermions are charged under this symmetry. However, Yukawa matrices can arise through non-renormalizable operators. The Higgs spectrum of these models includes the flavon, which could mix with the Higgs bosons when the flavor scale is of the order of the TeVs. The flavon phenomenology has been studied by several authors, including the production and decay processes  $pp \rightarrow H_F \rightarrow hh(h \rightarrow \gamma\gamma, h \rightarrow b\bar{b})$ ,  $pp \rightarrow H_F \rightarrow ZZ(Z \rightarrow \ell^-\ell^+)$ ,  $pp \rightarrow H_F \rightarrow tc(t \rightarrow \ell\nu_\ell b)$ ,  $pp \rightarrow H_F \rightarrow \tau\mu(\tau \rightarrow \ell\nu_\tau\nu_\ell)$  ( $\ell = e, \mu$ ) [9–13]. In this study, we explore a final state in which current experimental reports on searches for the di-Higgs boson can shed light on the signal we propose, i.e., the production of the flavon via proton-proton collisions and later it decays into  $b\bar{b}h$  for two particular channels, namely  $h \rightarrow b\bar{b}$  and  $h \rightarrow \gamma\gamma$ . The induced Feynman diagrams of the decay  $H_F \rightarrow f\bar{f}h$  in the theoretical framework of the FNSM are presented in Fig. 1<sup>1</sup>. The main difference between the di-Higgs boson production signatures and our signal is the resonant effect that offers the decay  $H_F \rightarrow b\bar{b}h$ . This is a great advantage from an experimental point of view.

The paper is organized as follows. Section II presents the relevant aspects of the model, including expressions for the masses and the Feynman rules to be used in the subsequent analysis. Afterwards, both theoretical and experimental constraints that have a direct impact on the predictions are studied in Sec. III. Meanwhile, Sec. IV is focused on the analysis of the signal,  $pp \rightarrow H_F \rightarrow hb\bar{b}$  ( $h \rightarrow b\bar{b}, \gamma\gamma$ ) as well as its background processes. A multivariate analysis is also included. Finally, we present our conclusions in Sec. V.

---

<sup>1</sup> The diagram (b) has a scalar propagator in which both the Higgs boson  $h$  and the flavon  $H_F$  propagate.

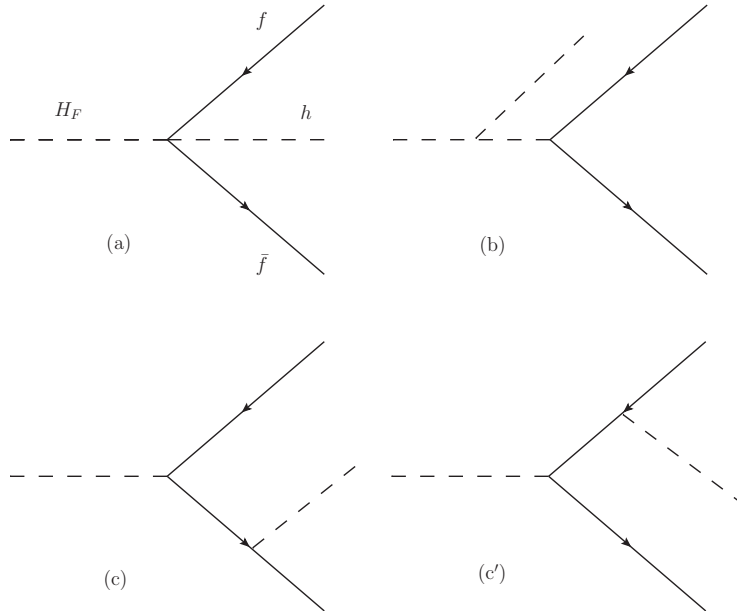


FIG. 1: Feynman diagrams inducing the  $H_F \rightarrow \bar{f}fh$  decay in the FNSM.

## II. THE MODEL

### A. The scalar sector

The FNSM's scalar sector add one complex singlet FN scalar  $S_F$  to the SM, namely,

$$S_F = \frac{(v_s + S_R + iS_I)}{\sqrt{2}}, \quad (2.1)$$

where  $v_s$  represents the vacuum expectation value (VEV) of the FN singlet. The scalar potential is invariant under the FN  $U(1)_F$  flavor symmetry. Under this flavor symmetry,  $S_F$  and the SM Higgs doublet  $\Phi = (\frac{v+\phi^0}{\sqrt{2}} \ \phi^+)^T$  transform as  $S_F \rightarrow e^{i\alpha} S_F$  and  $\Phi \rightarrow \Phi$ , respectively. We note that such a scalar potential allows a complex VEV,  $\langle S_F \rangle_0 = \frac{v_s}{\sqrt{2}} e^{i\alpha}$ , but in this work we assume the scenario in which the Higgs potential is CP-conserving ( $\alpha = 0$ ). Then, the CP-conserving Higgs potential reads:

$$V_0 = -\frac{1}{2}m_1^2\Phi^\dagger\Phi - \frac{1}{2}m_2^2S_F^*S_F + \frac{1}{2}\lambda_1(\Phi^\dagger\Phi)^2 + \lambda_2(S_F^*S_F)^2 + \lambda_3(\Phi^\dagger\Phi)(S_F^*S_F). \quad (2.2)$$

After the spontaneous symmetry breaking of the  $U(1)_F$  flavor symmetry by the VEVs of the spin-0 fields  $(\Phi, S_F)$ , a massless Goldstone boson will emerge in the physical spectrum. To give a mass to it, we embed a soft  $U(1)_F$  breaking term in the scalar potential:

$$V_{\text{soft}} = -\frac{m_3^2}{2}(S_F^2 + S_F^{*2}). \quad (2.3)$$

Thus, the full scalar potential is given by:

$$V = V_0 + V_{\text{soft}}. \quad (2.4)$$

The parameter  $\lambda_3$  in Eq.(2.2) allows a mixing between the Flavon and the Higgs fields after both the  $U(1)_F$  flavor and EW symmetries are spontaneously broken, generating the masses of the Flavon and Higgs field, as presented below while the pseudoscalar Flavon ( $S_I$ ) mass is generated via the soft  $U(1)_F$  flavor symmetry breaking term  $V_{\text{soft}}$ . Once the minimization of the potential  $V$  is done, we obtain relations between the parameters of  $V$  as follows:

$$m_1^2 = v^2 \lambda_1 + v_s^2 \lambda_3, \quad (2.5)$$

$$m_2^2 = -2m_3^2 + 2v_s^2 \lambda_2 + v^2 \lambda_3. \quad (2.6)$$

Since all parameters of the scalar potential are assumed to be real, the imaginary and real parts of  $V$  do not mix. The CP-even mass matrix can be written in the  $(\phi_0, S_R)$  basis as:

$$M_S^2 = \begin{pmatrix} \lambda_1 v^2 & \lambda_3 v v_s \\ \lambda_3 v v_s & 2\lambda_2 v_s^2 \end{pmatrix}, \quad (2.7)$$

whose mass eigenstates can be obtained through the following  $2 \times 2$  rotation:

$$\phi^0 = \cos \alpha h + \sin \alpha H_F, \quad (2.8)$$

$$S_R = -\sin \alpha h + \cos \alpha H_F, \quad (2.9)$$

where  $\alpha$  is the mixing angle. We identify  $h$  with the SM-like Higgs boson with mass  $M_h = 125.5$  GeV. Meanwhile, the mass eigenstate  $H_F$  is identified with the CP-even Flavon. The CP-odd Flavon  $A_F \equiv S_I$  will obtain its mass from the  $V_{\text{soft}}$  term such that  $M_{A_F}^2 = 2m_3^2$ . We will work (as free parameters) with the physical masses  $M_S$  ( $S = h, H_F, A_F$ ) and the mixing angle  $\alpha$ , whose relations with the quartic couplings of the scalar potential in Eq. (2.2) read:

$$\begin{aligned} \lambda_1 &= \frac{\cos^2 \alpha M_h^2 + \sin^2 \alpha M_{H_F}^2}{v^2}, \\ \lambda_2 &= \frac{M_{A_F}^2 + \cos^2 \alpha M_{H_F}^2 + \sin^2 \alpha M_h^2}{2v_s^2}, \\ \lambda_3 &= \frac{\cos \alpha \sin \alpha}{v v_s} (M_{H_F}^2 - M_h^2). \end{aligned} \quad (2.10)$$

TABLE I: Diagonal  $SXX$  interactions, ( $S = h, H_F, A_F$ ).

Vertex $SXX$	Coupling
$hf_i\bar{f}_i$	$\frac{v_s m_f}{v\Lambda^2} (v \sin \alpha - v_s \cos \alpha)$
$hZZ$	$g_{cW}^{m_Z} \cos \alpha$
$hWW$	$gm_W \cos \alpha$
$H_F f_i \bar{f}_i$	$-\frac{v_s m_f}{v\Lambda^2} (v_s \sin \alpha + v \cos \alpha)$
$H_F ZZ$	$g_{cW}^{m_Z} \sin \alpha$
$H_F WW$	$gm_W \sin \alpha$
$A_F f_i \bar{f}_i$	$-\frac{v_s m_f}{\Lambda^2}$
$A_F ZZ$	0
$A_F WW$	0

### B. The Yukawa sector

The effective  $U(1)_F$  invariant Yukawa Lagrangian includes terms that become the Yukawa couplings after the  $U(1)_F$  flavor symmetry is spontaneously broken. It is given by [8]:

$$\begin{aligned}
\mathcal{L}_Y = & \rho_{ij}^d \left( \frac{S_F}{\Lambda} \right)^{q_{ij}^d} \bar{Q}_i d_j \tilde{\Phi} + \rho_{ij}^u \left( \frac{S_F}{\Lambda} \right)^{q_{ij}^u} \bar{Q}_i u_j \Phi \\
& + \rho_{ij}^\ell \left( \frac{S_F}{\Lambda} \right)^{q_{ij}^\ell} \bar{L}_i \ell_j \Phi + \text{h.c.},
\end{aligned} \tag{2.11}$$

where  $\rho_{ij}^f$  ( $f = u, d, \ell$ ) are dimensionless parameters ostensibly of order  $\mathcal{O}(1)$ . The amounts  $q_{ij}^f$  represent the Abelian charges that reproduce the observed fermion masses and  $\Lambda$  is the ultraviolet mass scale, which is not predicted by the Froggat-Nielsen mechanism, it can be between the weak and the Planck scale. However, there is an essential requirement: the flavor symmetry must be broken in a way such that the ratio  $\frac{v_s}{\sqrt{2}\Lambda} \lesssim 1$ . To generate the Yukawa couplings from Lagrangian (2.11) one must spontaneously break both, the  $U(1)_F$  as well as EW symmetries. Once this is done, we arrive to the  $Sf_i\bar{f}_i$  interactions as shown in Table I. We note that to avoid large deviations from the SM coupling,  $v_s \approx \Lambda$  and  $\cos \alpha \approx -1$  are required, as below.

The CP-even  $H_F$  and the CP-odd  $A_F$  flavons are assumed to be heavier than  $h$ .

Meanwhile, to induce non-diagonal  $Sf_i\bar{f}_j$  interactions, we proceed as described below. By considering the unitary gauge one can make the following first order expansion of the neutral component of the heavy Flavon field  $S_F$  around its VEV  $v_s$ :

$$\begin{aligned}
\left( \frac{S_F}{\Lambda} \right)^{q_{ij}} &= \left( \frac{v_s + S_R + iS_I}{\sqrt{2}\Lambda} \right)^{q_{ij}} \\
&\simeq \left( \frac{v_s}{\sqrt{2}\Lambda} \right)^{q_{ij}} \left[ 1 + q_{ij} \left( \frac{S_R + iS_I}{v_s} \right) \right],
\end{aligned} \tag{2.12}$$

which leads to the following Lagrangian interaction after replacing the mass eigenstates:

$$\begin{aligned}
\mathcal{L}_Y &= \frac{1}{v} [\bar{U} M^u U + \bar{D} M^d D + \bar{L} M^\ell L] (c_\alpha h + s_\alpha H_F) \\
&+ \frac{v}{\sqrt{2} v_s} [\bar{U}_i \tilde{Z}_{ij}^u U_j + \bar{D}_i \tilde{Z}_{ij}^d D_j + \bar{L}_i \tilde{Z}_{ij}^\ell L_j] \\
&\times (-\sin \alpha h + \cos \alpha H_F + i A_F) + \text{h.c.},
\end{aligned} \tag{2.13}$$

Here,  $M^f$  denotes the diagonal fermion mass matrix. We encapsulate the Higgs-Flavon couplings in the  $\tilde{Z}_{ij}^f = U_L^f Z_{ij}^f U_L^{f\dagger}$  matrices. In the flavor basis, the  $Z_{ij}^f$  matrix elements are given by:

$$Z_{ij}^f = \rho_{ij}^f \left( \frac{v_s}{\sqrt{2}\Lambda} \right)^{q_{ij}^f} q_{ij}^f, \tag{2.14}$$

which (in general) remains non-diagonal even after diagonalizing the mass matrices, giving rise to FV interactions.

Finally, in addition to the Yukawa couplings, we also need the  $H_F h f_i \bar{f}_j$  couplings for our calculations. In the FNSM these interactions are given by

$$H_F h f \bar{f} = \frac{m_f v_s}{\sqrt{2}\Lambda^2} (1 - 2 \cos^2 \alpha). \tag{2.15}$$

As a particular case we will explore the scenario where  $f = b$ . This choice is motivated by experimental reports on Higgs pair searches [3–7]

### III. CONSTRAINTS ON THE FNSM PARAMETER SPACE

In order to compute a realistic numerical analysis of the signals proposed in this project, i.e.,  $pp \rightarrow H_F \rightarrow h b \bar{b}$  ( $h \rightarrow b \bar{b}, \tau^- \tau^+, WW^*, \gamma\gamma, ZZ^*$ ), we need to constrain the free FNSM parameters involved in the upcoming calculations, namely,

- The mixing angle  $\alpha$  of the real components of the doublet  $\Phi$  and the FN singlet  $S$ ,
- FN singlet VEV  $v_s$ ,
- The ultraviolet mass scale  $\Lambda$ ,
- CP-even scalar mass  $M_{H_F}$ .

These parameters can be constrained by several types of theoretical restrictions like absolute vacuum stability, triviality, perturbativity, and unitarity of scattering matrices and different experimental data, mainly, LHC Higgs boson data upper limits on the production cross-section of additional Higgs states. We also consider bounds on Lepton Flavor Violating processes (LFVp)

$L_i \rightarrow \ell_j \ell_k \bar{\ell}_k, \ell_i \rightarrow \ell_j \gamma$ . Measurements on  $\mathcal{BR}(B_{s,d}^0 \rightarrow \mu^+ \mu^-)$  and the anomalous magnetic moments of the muon and electron  $\Delta a_\mu$  and  $\Delta a_e$ , respectively, are also presented. Finally, we also take into account quark flavor constraints:  $B - \bar{B}$ ,  $K - \bar{K}$  and  $D - \bar{D}$  mixing.

## A. theoretical constraints

### 1. Stability of the scalar potential

It is necessary to control the stability of the scalar potential in Eq. (2.2), it should be bounded from below, i.e., it should not approach negative infinity along any direction of the field space  $(h, H_F, A_F)$  at large field values. The quadratic terms in the scalar potential are very suppressed compared to the quartic terms. So, the absolute stability conditions read [14]:

$$\left( \lambda_1, \lambda_2, \lambda_3 + \sqrt{2\lambda_1\lambda_2} \right) > 0. \quad (3.1)$$

The quartic couplings are evaluated at a scale  $\Lambda$  using the Renormalization Group Evolution (RGE) equations. If the scalar potential in Eq. (2.2) has a metastable EW vacuum, then these conditions should be modified [14]. To constrain the scalar field masses  $M_\phi$ , the VEV of the complex singlet  $v_s$  and the mixing angle  $\alpha$ , we can use Eqs. (2.10) to translate these limits into those on the model parameters.

### 2. Perturbativity and unitarity constraints

The upper limits are presented in Eq. (3.2) are necessary to ensure that the radiatively corrected scalar potential of the FNSM remains perturbative at any energy scale:

$$|\lambda_1, \lambda_2, \lambda_3| \leq 4\pi. \quad (3.2)$$

The quartic couplings that come from the scalar potential are also highly constrained by the unitarity of the  $S$ -matrix. Even at large field values, one can obtain the  $S$ -matrix by considering several  $(P)S - (P)S$ ,  $V - V$  and  $(P)S - V$  interactions in  $2 \rightarrow 2$  body processes, where  $P(S, V)$  stands for a pseudo-scalar boson (scalar, gauge boson). The unitarity of the  $S$ -matrix demands that its eigenvalues be less than  $8\pi$  [14, 15]. Within the theoretical framework of FNSM, using the equivalence theorem, the unitary bounds are given by:

$$\lambda_1 \leq 16\pi \quad \text{and} \quad \left| \lambda_1 + \lambda_2 \pm \sqrt{(\lambda_1 - \lambda_2)^2 + (2/3\lambda_3)^2} \right| \equiv |\lambda_U^\pm| \leq 16/3\pi. \quad (3.3)$$

By using the Eqs. (2.10), (3.2) and (3.3), we can constrain the scalar singlet VEV  $v_s$ , the heavy Higgs masses  $(M_{H_F}, M_{A_F})$  and the mixing angle  $\alpha$ .

Figure 2 displays the  $\cos \alpha - v_s$  plane whose points represent those allowed by the theoretical

TABLE II: Scanned parameters.

Parameter	Interval
$\cos \alpha$	$[-1, 1]$
$M_{H_F}$	800-1500 GeV
$M_{A_F}$	800-1500 GeV
$v_s$	$v$ -5000 GeV

constraints, perturbativity and unitarity of the  $S$ -matrix. For this purpose we generate random points such that they meet the relations (2.10), (3.2) and (3.3). We present in Table II the scanned intervals to achieve that proposal.

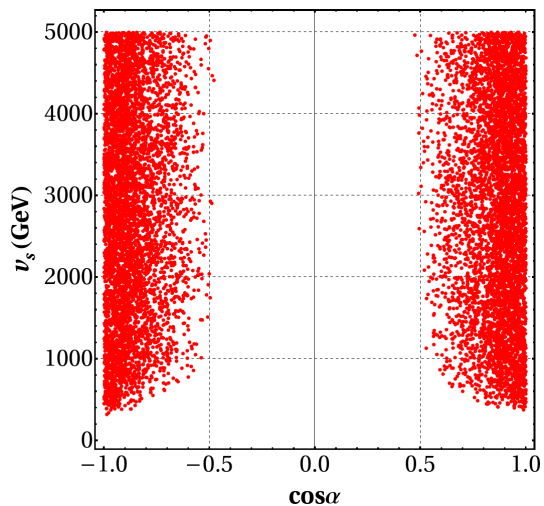


FIG. 2: VEV of the FN singlet  $v_s$  as a function of cosine of the mixing angle  $\alpha$ . The red points indicate those allowed by all theoretical restrictions as mentioned in the main text.

We find that  $|\lambda_U^+| \leq 16\pi/3$  is the most stringent upper bound for the scalar quartic couplings, which is transferred to a lower limit on the scalar singlet VEV  $v_s \geq (276, 345, 415, 519)$  GeV, for specific masses of  $M_{H_F} = M_{A_F} = (800, 1000, 1200, 1500)$  GeV and  $\cos \alpha = -0.995$ . Note that we are working at the EW scale only, as detailed RGE analysis is beyond the scope of this work. We also observe a greater density around 1 and  $-1$ , this is because  $\alpha$  must tend to zero so as not to have large deviations from the  $hf\bar{f}$  coupling of the SM.

It is important to highlight that the masses were analyzed in the range shown in Table II because in a previous study by one of us (and others)[11], it was found that  $M_{H_F} > 800$  GeV to release the limit on the cross-section of the process  $pp \rightarrow S \rightarrow hh$  reported by the ATLAS Collaboration [16], where  $S$  is a resonant (pseudo-)scalar particle.



TABLE III: Scanned parameters.

Parameter	Interval
$\cos \alpha$	[-1, -0.7]
$\Lambda$	$v$ -5000 GeV
$v_s$	$v$ -5000 GeV

## B. Experimental constraints

### 1. LHC Higgs boson data

We complement the theoretical constraints by using experimental measurements of Higgs boson physics [17], specifically we consider the *signal strengths* defined as

$$\mathcal{R}_X = \frac{\sigma(pp \rightarrow h) \cdot \mathcal{BR}(h \rightarrow X)}{\sigma(pp \rightarrow h^{\text{SM}}) \cdot \mathcal{BR}(h^{\text{SM}} \rightarrow X)}, \quad (3.4)$$

where  $\sigma(pp \rightarrow H_i)$  is the production cross-section of  $H_i$ , with  $H_i = h, h^{\text{SM}}$ ; here  $h$  is the SM-like Higgs boson coming from an extension of the SM and  $h^{\text{SM}}$  is the SM Higgs boson;  $\mathcal{BR}(H_i \rightarrow X)$  is the branching ratio of the decay  $H_i \rightarrow X$ , with  $X = b\bar{b}, c\bar{c}, \tau^-\tau^+, \mu^-\mu^+, WW^*, ZZ^*, \gamma\gamma$ .

### 2. Lepton Flavor Violating processes

Furthermore, we also analyze several LFVp that can help us even more in constraining the parameters involved in subsequent calculations. Specifically, we use i) upper limits on  $\mathcal{BR}(L_i \rightarrow \ell_j \ell_k \bar{\ell}_k)$  and  $\mathcal{BR}(\ell_i \rightarrow \ell_j \gamma)$ , ii) measurements on  $\mathcal{BR}(B_{s,d}^0 \rightarrow \mu^+ \mu^-)$  and the anomalous magnetic moments of the muon  $\Delta a_\mu$ . We also analyze the upper-limit on  $\mathcal{BR}(h \rightarrow \ell_i \ell_j)$  [18, 19]. However, we find it is not enough restricted. We implement the model in the `Mathematica` package so-called `SpaceMath` [20] to analyze the FNSM parameter space. We present in Fig. 3 the ultraviolet mass scale  $\Lambda$  as a function of the VEV of the complex singlet  $v_s$ . The different points represent individual  $\mathcal{R}'_X$ s; the blue circles (green triangles, yellow diamonds, green squares, orange triangles, green rectangles) correspond to  $\mathcal{R}_W$  ( $\mathcal{R}_Z, \mathcal{R}_\gamma, \mathcal{R}_\tau, \mathcal{R}_b$ ). The common region of all them is represented by the enclosed area in solid black lines. The green rectangle stands for the allowed area by all the LFVp<sup>2</sup>. Meanwhile, the cyan area is the result of applying all discussed theoretical and experimental constraints (intersection). Motivated by the analysis done in Sec. III A 2, we again scan on the model's parameters involved in the evaluation of the  $\mathcal{R}_X$ 's, as shown in Table III. We also have explored the allowed values by  $\mathcal{R}_{\mu,c}$  (not presented in Fig. 3), however, these measurements are not very stringent in the FNSM. It is worth to highlight the fact  $v_s \approx \Lambda$ , this

<sup>2</sup> According to our analysis, the upper bound on  $\Lambda$  and  $v_s$  is imposed by the anomalous magnetic moment of the muon. However, the situation could change because is still possible that more precise determinations of the SM hadronic contribution and the experimental measurement would settle the discrepancy in the future without requiring any new physics effects.

is to be expected because the coupling  $h f \bar{f}$  behaves as  $v_s^2/\Lambda^2$  for  $\cos \alpha \approx -1$ , as shown in Table I.

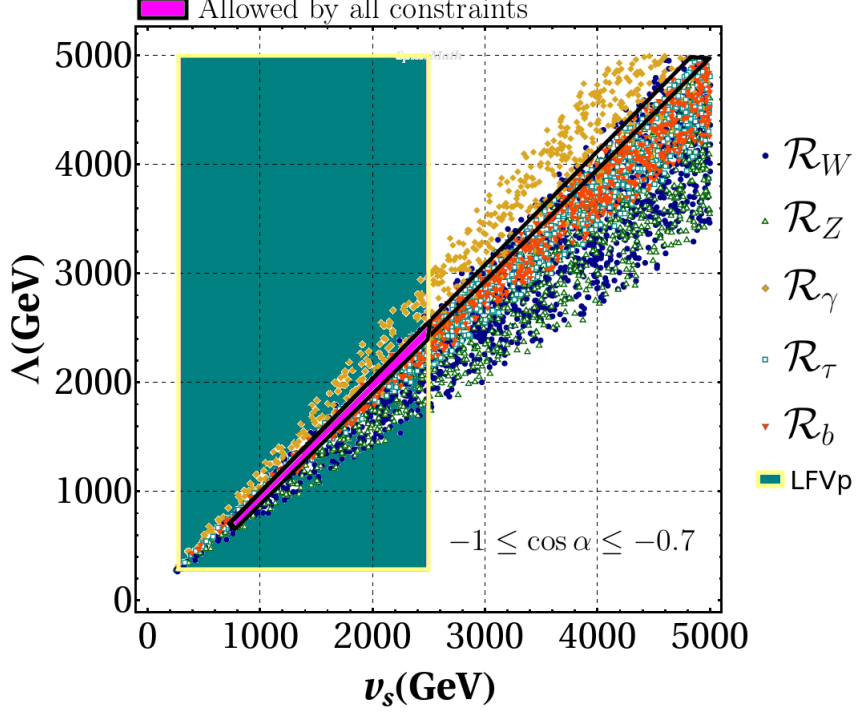


FIG. 3: Ultraviolet mass scale  $\Lambda$  as a function of the VEV of the complex singlet  $v_s$ . The different points represent individual  $\mathcal{R}'_X$ s, while the enclosed area by solid black lines is the common zone of them. The green rectangle stands for the allowed region by LFVp. Meanwhile, the cyan area is the result of applying all discussed theoretical and experimental constraints (intersection).

### 3. Neutral meson mixing

The effective Hamiltonian describing  $\Delta F = 2$  interactions is given by

$$\begin{aligned} \mathcal{H}_{eff}^{\Delta F=2} = & C_1^{ij} (\bar{q}_L^i \gamma_\mu q_L^j)^2 + \tilde{C}_1^{ij} (\bar{q}_R^i \gamma_\mu q_R^j)^2 + C_2^{ij} (\bar{q}_R^i q_L^j)^2 \\ & + \tilde{C}_2^{ij} (\bar{q}_L^i q_R^j)^2 + C_4^{ij} (\bar{q}_R^i q_L^j) (\bar{q}_L^i q_R^j) + C_5^{ij} (\bar{q}_L^i \gamma_\mu q_L^j) (\bar{q}_R^i \gamma^\mu q_R^j) + \text{h.c.} \end{aligned} \quad (3.5)$$

At tree level, flavon exchange leads to the generation of Wilson coefficients[21, 22]

$$\begin{aligned} C_2^{ij} &= -(g_{ji}^*)^2 \left( \frac{1}{m_s^2} - \frac{1}{m_a^2} \right) \\ \tilde{C}_2^{ij} &= -g_{ij}^2 \left( \frac{1}{m_s^2} - \frac{1}{m_a^2} \right) \end{aligned}$$

$$C_4^{ij} = -\frac{g_{ij}g_{ji}}{2} \left( \frac{1}{m_s^2} + \frac{1}{m_a^2} \right). \quad (3.6)$$

For  $M_{A_F} = M_{H_F}$  the two contributions to  $C_2$  and  $\tilde{C}_2$  cancel, whereas constructive interference can be generated via the Wilson coefficient  $C_4$ .

### *K – $\bar{K}$ mixing*

The limits from  $K – \bar{K}$  mixing at 95% C.L. [23] are given by

$$C_{\epsilon_K} = \frac{\text{Im}\langle K^0 | \mathcal{H}^{\Delta F=2} | \bar{K}^0 \rangle}{\text{Im}\langle K^0 | \mathcal{H}_{\text{SM}}^{\Delta F=2} | \bar{K}^0 \rangle} = 1.12_{-0.25}^{+0.27}; \quad C_{\Delta m_K} = \frac{\text{Re}\langle K^0 | \mathcal{H}^{\Delta F=2} | \bar{K}^0 \rangle}{\text{Re}\langle K^0 | \mathcal{H}_{\text{SM}}^{\Delta F=2} | \bar{K}^0 \rangle} = 0.93_{-0.42}^{+1.14}$$

The contributions of SM and flavon are included in  $\mathcal{H}^{\Delta F=2}$ , while  $\mathcal{H}_{\text{SM}}^{\Delta F=2}$  represents the contribution of SM. The observed dip characteristic arises from the accidental cancellation that occurs in  $C_2^{sd}$  and  $\tilde{C}_2^{sd}$ , as shown in the Wilson coefficients generated by flavon exchange at tree-level [21, 22]. This feature is universally observed within in  $K – \bar{K}$  mixing. However, it is absent in the specific scenarios where the contribution to  $C_4^{sd}$  becomes so dominant that it overshadows all other contributions.

### *B – $\bar{B}$ mixing*

For both variations of  $B – \bar{B}$  mixing, it is defined as follows,

$$C_{B_q} e^{2i\varphi_{B_q}} = \frac{\langle B_q | \mathcal{H}^{\Delta F=2} | \bar{B}_q \rangle}{\langle B_q | \mathcal{H}_{\text{SM}}^{\Delta F=2} | \bar{B}_q \rangle}, \quad (3.7)$$

with the 95% CL limits [23] given by

$$\begin{aligned} C_{B_d} &= 1.05 \pm 0.11, & \varphi_{B_d} &= -2.0 \pm 1.8, \\ C_{B_s} &= 1.110 \pm 0.090, & \varphi_{B_s} &= 0.42 \pm 0.89. \end{aligned} \quad (3.8)$$

### *D – $\bar{D}$ mixing*

Given that the SM contribution to the  $D – \bar{D}$  mixing process is significantly affected by substantial hadronic uncertainties, it is recommended to define and restrict the contributions of flavons ensuring that they do not exceed the constraint  $2\sigma$ [24].

$$|M_{12}^D| = |\langle D | \mathcal{H}^{\Delta F=2} | \bar{D} \rangle| < 7.5 \times 10^{-3} \text{ ps}^{-1}. \quad (3.9)$$

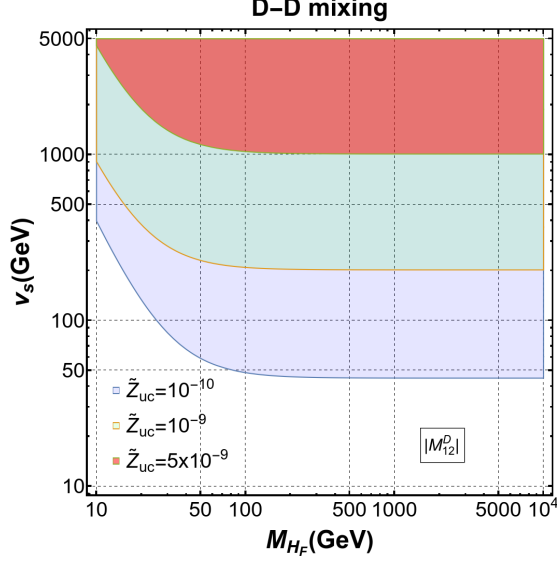


FIG. 4:  $M_{H_F} - v_s$  plane showing the region allowed due to flavon contributions to  $|M_{12}^D|$ . Blue area:  $\tilde{Z}_{uc}=10^{-10}$ , green area:  $\tilde{Z}_{uc}=10^{-9}$ , red area:  $\tilde{Z}_{uc}=5 \times 10^{-9}$ .

In Refs. [9, 25] are presented stringent restrictions in the  $v_s - M_{A_F}$  plane that come from mixtures of mesons. However, we evade them by inheriting them to the parameters  $\tilde{Z}_{ds}$ ,  $\tilde{Z}_{db}$  and  $\tilde{Z}_{uc}$  for  $K - \bar{K}$ ,  $B - \bar{B}$  and  $D - \bar{D}$ , respectively. We presented in Fig. 4 the  $M_{H_F} - v_s$  plane for three different values of  $\tilde{Z}_{uc}$ ;  $10^{-10}$ ,  $10^{-9}$  and  $5 \times 10^{-9}$ . The colored areas are these allowed by  $|M_{12}^D|$ . Similar constraints are obtained for  $K - \bar{K}$  and  $B - \bar{B}$ .

#### IV. COLLIDER ANALYSIS

We first present the decay width  $\Gamma(H_F \rightarrow h\bar{f}f)$  of the three-body process in which we are interested. The study of these kinds of processes is interesting as it can also have a sizable branching ratio. The Feynman diagrams that contribute to these reactions are shown in Fig. 1.

The decay width can be written as follows

$$\Gamma(H_F \rightarrow h\bar{f}f) = \frac{M_{H_F}}{256\pi^3} \int dx_a \int dx_b |\overline{\mathcal{M}}|^2, \quad (4.1)$$

where the average square amplitude is given by

$$\begin{aligned} |\overline{\mathcal{M}}|^2 &= \frac{1}{2(x_a + x_b + x_h - 2)^2} (x_a + x_b + x_h - 4x_t - 1) ((x_a + x_b + x_h - 2)C_a + C_b)^2 \\ &+ \frac{2}{(x_a - 1)^2 (x_b - 1)^2} \left( (x_a - 1)(x_b - 1)(x_a - x_b)^2 - 16(x_a + x_b - 2)^2 x_t^2 \right) \end{aligned}$$

$$\begin{aligned}
& + 4(x_a + x_b - 2)(2 - 3x_b + x_a(4x_b - 3))x_t + x_h(4(x_a + x_b - 2)^2x_t - (x_a - x_b)^2) \Big) C_c^2 \\
& - \frac{4\sqrt{x_t}}{(x_a - 1)(x_b - 1)}(x_a^2 + 2(3x_b + x_h - 4x_t - 3)x_a + x_b^2 - 4x_h + 2x_b(x_h - 4x_t - 3) \\
& + 16x_t + 4)C_aC_c - \frac{4\sqrt{x_t}}{(x_a - 1)(x_b - 1)(x_a + x_b + x_h - 2)} \left( x_a^2 + 2(3x_b + x_h - 4x_t - 3)x_a \right. \\
& \left. + x_b^2 - 4x_h + 2x_b(x_h - 4x_t - 3) + 16x_t + 4 \right) C_bC_c. \tag{4.2}
\end{aligned}$$

with  $x_a = (m_a/M_{H_F})^2$ . The factors  $C_a = g_{H_F h f f}$ ,  $C_b = g_{H_F h h} g_{h f f}/m_h^2$ , and  $C_c = g_{H_F f f} g_{h f f}/m_h$  are the coupling constants involved in the Feynman diagrams of Fig. 1. Finally, the integration domain is given by

$$2\sqrt{x_t} \leq x_a \leq 1 - x_h - 2\sqrt{x_t x_h}, \tag{4.3}$$

$$x_b \begin{matrix} \geq \\ \leq \end{matrix} \frac{2(1 - x_h + 2x_t) + x_a(x_a + x_h - 2x_t - 3) \mp \sqrt{x_a^2 - 4x_t} \sqrt{(x_a + x_h - 1)^2 - 4x_h x_t}}{2(1 - x_a + x_t)} \tag{4.4}$$

Meanwhile, the production cross-section of the heavy CP-even Flavon  $H_F$  (or pseudo scalar  $A_F$ , for that matter) depends mainly on the  $g_{H_F t \bar{t}} = \frac{c_\alpha v + s_\alpha v_s}{v_s} \frac{y_t}{\sqrt{2}}$  ( $g_{A_F t \bar{t}} = \frac{v}{v_s} \frac{y_t}{\sqrt{2}}$ ) coupling. The corresponding term in the effective Lagrangian reads [26]:

$$\mathcal{L}_{\text{eff}} = \frac{1}{v} g_{hgg} h G_{\mu\nu} G^{\mu\nu}, \tag{4.5}$$

$$g_{Sgg} = -i \frac{\alpha_S}{8\pi} \tau (1 + (1 - \tau) f(\tau)) \quad \text{with} \quad \tau = \frac{4M_t^2}{M_h^2}, \tag{4.6}$$

$$f(\tau) = \begin{cases} (\sin^{-1} \sqrt{\frac{1}{\tau}})^2, & \tau \geq 1, \\ -\frac{1}{4} [\ln \frac{1 + \sqrt{1 - \tau}}{1 - \sqrt{1 - \tau}} - i\pi]^2 & \tau < 1. \end{cases} \tag{4.7}$$

In FNSM, the  $ggh$ ,  $ggH_F$  and  $ggA_F$  couplings are given, respectively, by:

$$\begin{aligned}
g_{hgg} &= \left( \frac{c_\alpha v_s - s_\alpha v}{v_s} \right) g_{Sgg}, \\
g_{H_F gg} &= \left( \frac{c_\alpha v + s_\alpha v_s}{v_s} \right) g_{Sgg}, \\
g_{A_F gg} &= \frac{v}{v_s} (-i \alpha_S / \pi) \tau f(\tau), \tag{4.8}
\end{aligned}$$

$A_F$  is a CP-odd scalar and  $h, H_F$  are CP-even scalars so, once the couplings with left and right fields are written in terms of Dirac fields, the Hermitian part of the coupling in Eq. 2.11 gives rise to an  $i = \sqrt{-1}$  coupling for  $h, H_F$  and a  $\gamma_5$  coupling for  $A_F$ : so the result of the top quark loop integral is different for  $h, H_F$  and  $A_F$  [27, 28]. It is to be noted that, for  $M_{H_F, A_F} > 2M_t$ ,

$$f(\tau) = -\frac{1}{4}[\ln \frac{1+\sqrt{1-\tau}}{1-\sqrt{1-\tau}} - i\pi]^2.$$

As far as our computation scheme is concerned, we first use `FeynRules` [29] to obtain the FNSM model and produce the UFO files for `MadGraph-2.6.5` [30]. Using the ensuing particle spectrum in `MadGraph-2.6.5`, we calculate the production cross-section of the aforementioned production and decay process. The `MadGraph_aMC@NLO` [30] framework has been used to generate the background events in the SM. The showering and hadronization simulations were performed with `Pythia-8` [31]. The detector response has been emulated using `Delphes-3.4.2` [32]. The default ATLAS card which comes along with the `Delphes-3.4.2` package was considered in this analysis. For both the signal and background processes, we consider the Leading Order (LO) cross-sections computed by `MadGraph_aMC@NLO`.

Once we have put on the table the way in which we evaluate the collider observables, we define in Table IV three scenarios to be studied in the following analysis.

TABLE IV: Scenarios (**S1**, **S2**, **S3**) used in the calculations.

Parameter	<b>S1</b>	<b>S2</b>	<b>S3</b>
$\cos \alpha$	0.995	0.995	0.995
$\Lambda$	1 TeV	1.5 TeV	2.5 TeV
$v_s$	1 TeV	1.5 TeV	2.5 TeV

We present in Table V the numerical cross-section of the proposed signal and the number of events produced by considering scenarios **S1**, **S2**, **S3**.

TABLE V: Cross-section of the signal for scenarios **S1**, **S2**, **S3**.

Scenario	$M_{H_F}$ (GeV)	$\sigma(pp \rightarrow H_F \rightarrow hb\bar{b})$ (fb)	Events ( $\mathcal{L}_{\text{int}} = 300\text{fb}^{-1}$ )
<b>S1</b>	(800, 900, 1000)	(6.8, 3.3, 1.7)	(2040, 990, 510)
<b>S2</b>	(800, 900, 1000)	(4.3, 2.3, 1.3)	(1290, 690, 390)
<b>S3</b>	(800, 900, 1000)	(3.8, 2.1, 1.1)	(1140, 630, 330)

Meanwhile, Fig. 5 presents an overview of the production cross-section of the signal  $pp \rightarrow H_F \rightarrow hb\bar{b}$  by considering the three scenarios **S1**, **S2**, **S3**.

On the other hand, we analyze two particular channels in which the Higgs boson decays, namely, i)  $pp \rightarrow H_F \rightarrow hb\bar{b}(h \rightarrow b\bar{b})$  and ii)  $pp \rightarrow H_F \rightarrow hb\bar{b}(h \rightarrow \gamma\gamma)$ . The  $b$ -tagging of jets produced from the fragmentation and hadronization of bottom quarks represents a fundamental role in separating the signal from the background processes, which involve gluons, light-flavor jets ( $u$ ,  $d$ ,  $s$ ) and  $c$ -quark fragmentation. To overcome this problem, we use the `FastJet` package [33] (via `MadAnalysis` [34]) and invoke the anti- $k_T$  algorithm [35]. We also include the  $b$ -tagging efficiency  $\epsilon_b = 90\%$ . The probability that a  $c$ -jet or any other light-jet  $j$  is mistagged as a  $b$ -jet are  $\epsilon_c = 5\%$  and  $\epsilon_j = 1\%$  [36], respectively.

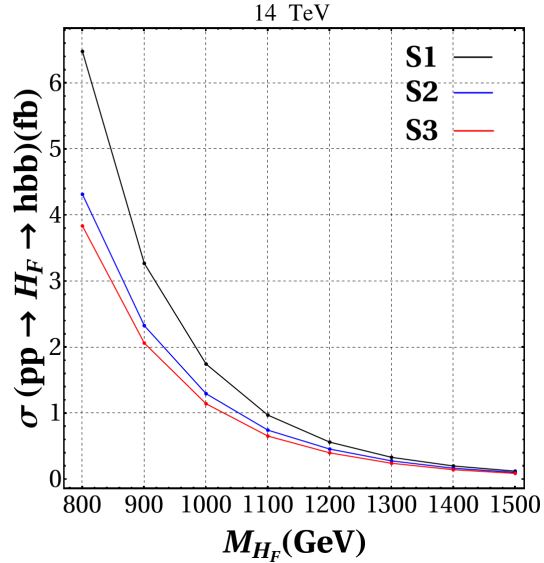


FIG. 5: Production cross-section of the signal  $pp \rightarrow H_F \rightarrow hbb$ . The centre-of-mass energy was set to 14 TeV.

TABLE VI: Cross-section of the SM background processes.

SM background process	Cross-section (fb)
$pp \rightarrow t\bar{t}$	26910
$pp \rightarrow Wh$	0.5463
$pp \rightarrow ZZ$	231.5
$pp \rightarrow Zh$	79.75
$pp \rightarrow \bar{b}bjj$	$5.441 \times 10^8$

1.  $pp \rightarrow H_F \rightarrow hbb(h \rightarrow b\bar{b})$

The SM background processes for the  $h \rightarrow b\bar{b}$  channel are given by

- $pp \rightarrow t\bar{t}$ , ( $t \rightarrow W^+b$ ,  $W^+ \rightarrow c\bar{b}$ ,  $\bar{t} \rightarrow W^-b$ ,  $W^+ \rightarrow b\bar{c}$ ),
- $pp \rightarrow Wh$ , ( $W \rightarrow cb$ ,  $h \rightarrow b\bar{b}$ ),
- $pp \rightarrow ZZ$ , ( $Z \rightarrow b\bar{b}$ ,  $Z \rightarrow b\bar{b}$ ),
- $pp \rightarrow Zh$ , ( $Z \rightarrow b\bar{b}$ ,  $h \rightarrow b\bar{b}$ ),
- $pp \rightarrow \bar{b}bjj$ , where  $j$  denotes non-bottom-quark jets.

The numerical cross-section of the SM background processes is presented in Table VI.

For this channel, the  $b$ -jets emerging from the primary vertex are expected to have a high transverse momentum  $p_T(b_1, b_2)$ , while these produced via the decay  $h \rightarrow b\bar{b}$  have a lower trans-

verse momentum than the primary ones  $p_T(b_3, b_4)$ . An important fact, and the clearest signature of our signal, is the resonant effect coming from the decay  $H_F \rightarrow h b \bar{b} (h \rightarrow b \bar{b}) \rightarrow b \bar{b} b \bar{b}$ .

We present in Fig. 6 the invariant mass  $M_{\text{inv}}(b_1 b_2 b_3 b_4)$  for scenario  $S1$  and  $M_{H_F} = 800$  GeV.

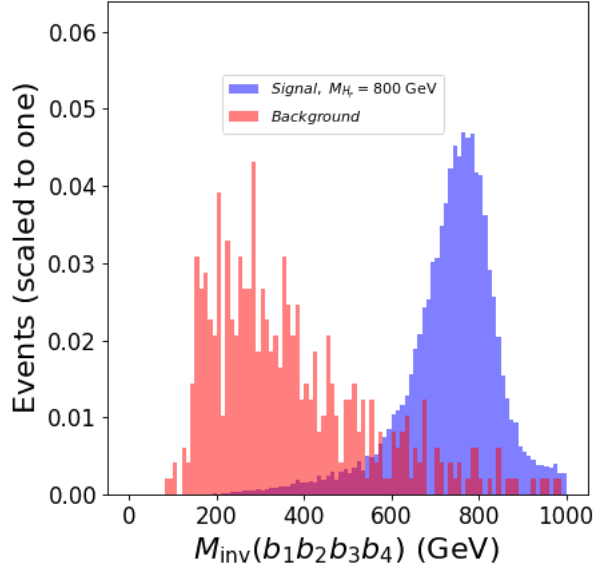


FIG. 6: Normalized distribution of the reconstructed invariant mass  $M_{\text{inv}}(b_1 b_2 b_3 b_4)$  for the signal and background processes.

Meanwhile, Fig. 7 shows the  $p_T(b_i)$  ( $i = 1, 2, 3, 4$ ) distribution including to the signal and the SM background processes. Subscript 1(4) corresponds to the  $b$ -jet with the highest (lowest) transverse momentum. While subscript 2(3) represents the second (third) dominant  $b$ -jet.

From Fig. 7 we note that  $p_T(b_1, b_2)$  are higher than  $p_T(b_3, b_4)$  because the former come from the primary vertex, while the last arise from the Higgs boson decay. Both  $p_T(b_i)$  and  $M_{\text{inv}}(b_1 b_2 b_3 b_4)$  are the most important variables to isolate the signal from the background.

## 2. $pp \rightarrow H_F \rightarrow h b \bar{b} (h \rightarrow \gamma \gamma)$

As far as the di-photon channel is concerned, the SM background processes are given by

- $pp \rightarrow ht\bar{t}, (h \rightarrow \gamma\gamma, t \rightarrow W^+ \bar{b}, W^+ \rightarrow \ell^+ \nu_\ell, \bar{t} \rightarrow W^- b, W^+ \rightarrow \ell^- \bar{\nu}_\ell),$
- $pp \rightarrow t\bar{t}\gamma\gamma, (t \rightarrow W^+ \bar{b}, W^+ \rightarrow \ell^+ \nu_\ell, \bar{t} \rightarrow W^- b, W^+ \rightarrow \ell^- \bar{\nu}_\ell),$
- $pp \rightarrow Wh, (W \rightarrow cb, h \rightarrow \gamma\gamma),$
- $pp \rightarrow Zh, (Z \rightarrow b\bar{b}, h \rightarrow \gamma\gamma),$
- $pp \rightarrow hjj, (h \rightarrow \gamma\gamma),$
- $pp \rightarrow \gamma\gamma jj$



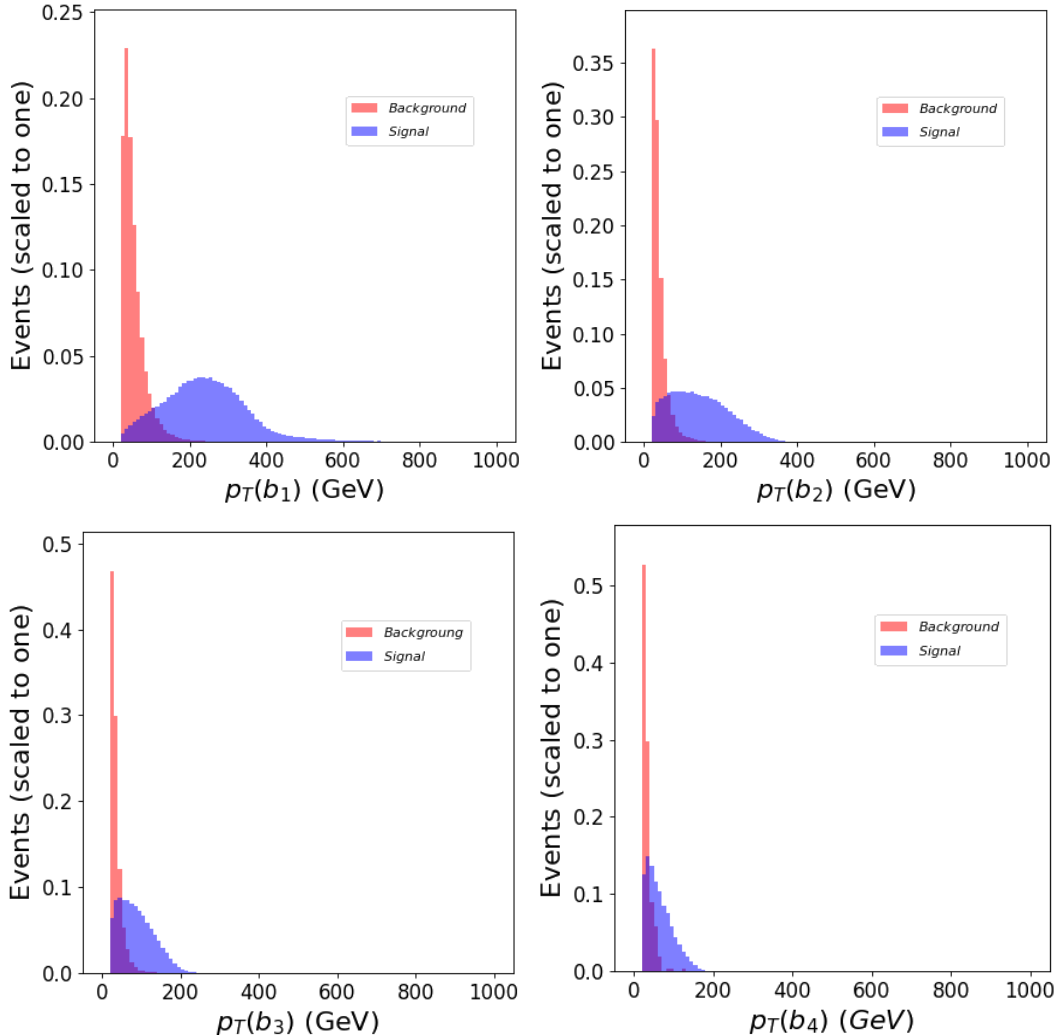


FIG. 7: Normalized distributions in  $b$ -jet transverse momentum for signal and total background after the acceptance cuts.

- $pp \rightarrow \gamma\gamma b\bar{b}$ .

The numerical cross-section of the SM background processes is presented in Table VII.

In this case we also have a similar scenario as in the previous channel concerning to the resonant effect coming from the decay  $H_F \rightarrow b\bar{b}\gamma\gamma$ . Figure 8 displays the invariant mass distribution  $M_{\text{inv}}(bb\gamma\gamma)$  for  $M_{H_F} = 900$  GeV. As in the previous channel, we also present in Fig. 9 the  $p_T(b_i)$ ,  $p_T(\gamma_i)$  ( $i = 1, 2$ ).

### A. Multivariate Analysis

After the kinematic analysis, we found that most of the observables used to distinguish signal from background have relatively weak discriminating power. Therefore, the final candidate selection is determined using Multivariate Analysis (MVA) discriminators, which combine these

TABLE VII: Cross-section of the SM background processes.

SM background processes	Cross-section (fb)
$pp \rightarrow ht\bar{t}$	$3.2 \times 10^{-2}$
$pp \rightarrow t\bar{t}\gamma\gamma$	0.57
$pp \rightarrow Wh$	$9.7 \times 10^{-4}$
$pp \rightarrow Zh$	0.14
$pp \rightarrow hjj$	13.62
$pp \rightarrow \gamma\gamma jj$	$1.1 \times 10^5$
$pp \rightarrow b\bar{b}\gamma\gamma$	5113

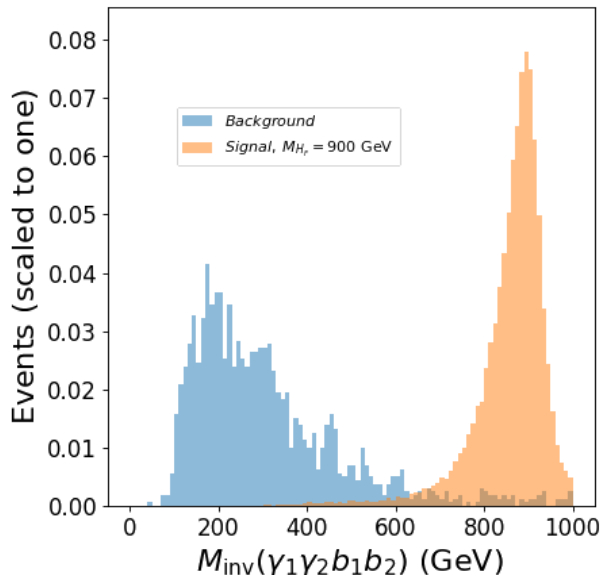


FIG. 8: Normalized distribution of the reconstructed invariant mass  $M_{\text{inv}}(\gamma_1\gamma_2b_1b_2)$  for the signal and background processes.

observables into a single, more powerful classifier. For the MVA training, we use a boosted decision tree (BDT) algorithm [37], implemented via the XGBoost library [38], which employs an advanced gradient boosting technique. The BDT classifiers are trained using variables related to the kinematics of final and intermediate state particles, including:

Case 1: Four  $b$ -jets ( $b_1, b_2, b_3, b_4$ ):

- Transverse momentum ( $p_T$ ):  $p_T(b_1), p_T(b_2), p_T(b_3), p_T(b_4)$
- Rapidity ( $\eta$ ):  $\eta(b_1), \eta(b_2), \eta(b_3), \eta(b_4)$
- Combined transverse momentum:  $p_T(b_1b_2b_3b_4)$

Case 2: Two  $b$ -jets ( $b_1, b_2$ ) and two photons ( $\gamma_1, \gamma_2$ ):

- Transverse momentum ( $p_T$ ):  $p_T(b_1), p_T(b_2), p_T(\gamma_1), p_T(\gamma_2)$

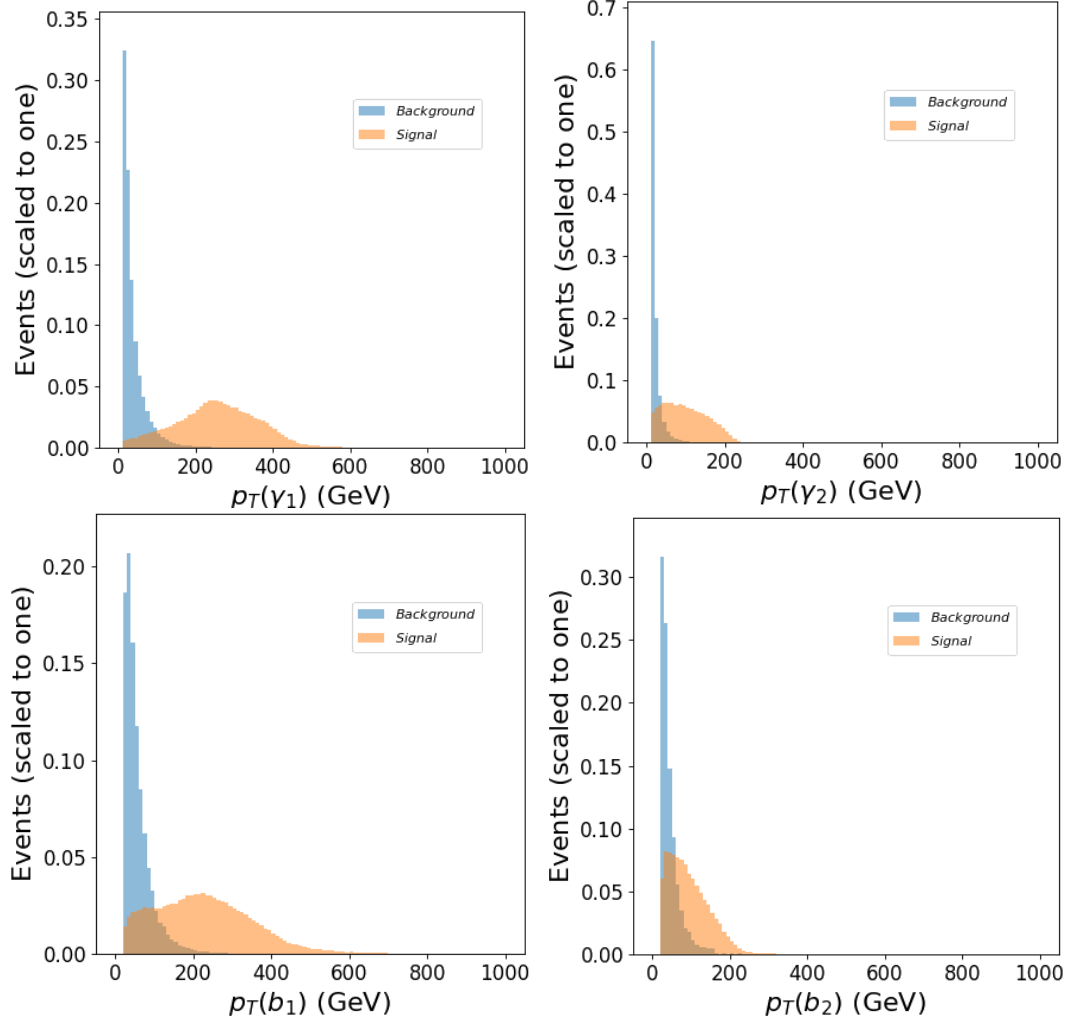


FIG. 9: Normalized distributions in  $b$ -jet and  $\gamma$  transverse momentum for signal and total background after the acceptance cuts.

- Rapidity ( $\eta$ ):  $\eta(b_1)$ ,  $\eta(b_2)$ ,  $\eta(\gamma_1)$ ,  $\eta(\gamma_2)$
- Invariant mass of the photons:  $M(\gamma_1\gamma_2)$
- Combined transverse momentum:  $p_T(b_1b_2b_3b_4)$

The BDT training is performed using the MC-simulated samples. The number of MC events are a dataset consisting of 200000 signal events and the samples of background events described above, each containing 200000 events. The data is split as follows: training dataset is 70% of the total events, while the testing dataset is 30% of the total events. To optimize the BDT model, we use *HyperOpt*[39] to tune the hyperparameters of the classifier. As an example of the performances of the trainings, Fig. 10 shows the plots for  $1/\text{Background Acceptance}$  against the  $\text{Signal Acceptance}$  for the  $h \rightarrow b\bar{b}$  channel.

These signal and background samples are scaled to the expected number of candidates, which is calculated based on the integrated luminosity and cross-sections. The BDT selection is opti-

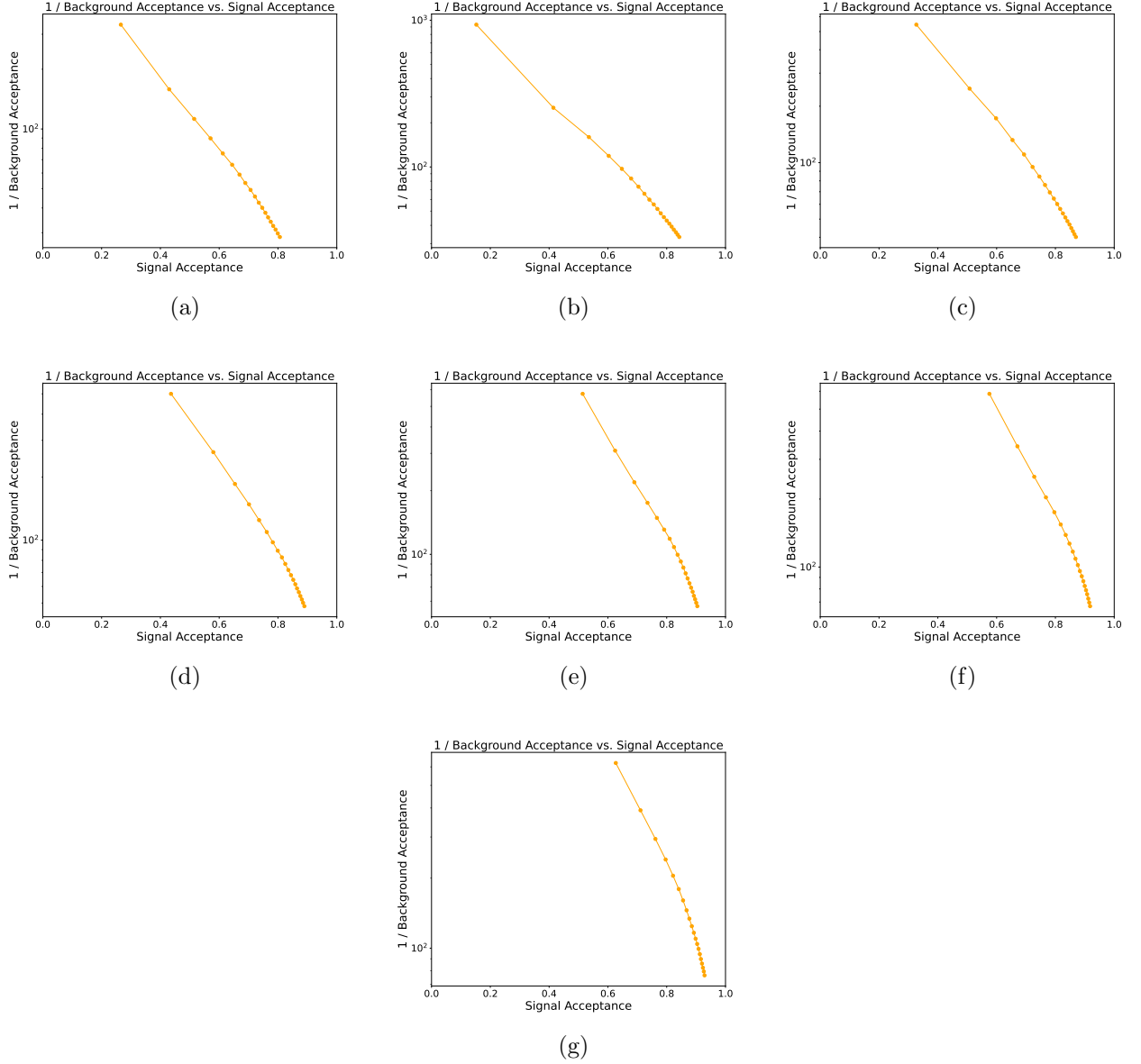


FIG. 10:  $1/\text{Background Acceptance}$  against the  $\text{Signal Acceptance}$  for  $h \rightarrow b\bar{b}$  channel. (a)  $M_{H_F} = 800$  GeV, (b)  $M_{H_F} = 900$  GeV, (c)  $M_{H_F} = 1000$  GeV, (d)  $M_{H_F} = 1100$  GeV, (e)  $M_{H_F} = 1200$  GeV, (f)  $M_{H_F} = 1300$  GeV and (g)  $M_{H_F} = 1400$  GeV.

mized individually for each channel to maximize the figure of merit, i.e., the *signal significance*, defined as  $S/\sqrt{S+B}$ , where  $S$  and  $B$  represent the number of signal and background candidates, respectively, in the signal region after applying the selection criteria.

In Fig. 11 we show the *signal significance* (for the three scenarios **Si**) as a function of the luminosity and the flavon mass  $M_{H_F}$  for the  $pp \rightarrow H_F \rightarrow hb\bar{b}(h \rightarrow b\bar{b})$  process. We observe that at a 14 TeV  $pp$  collider with an integrated luminosity of  $3000 \text{ fb}^{-1}$ , strong sensitivity exists for the various choices of  $M_{H_F}$ . We found that for the range  $800 < M_{H_F} < 950$  GeV a *signal significance* between  $3 - 5.6\sigma$  was obtained. Thus, with the arrival of the future HL-LHC, the flavon particle

could be discovered if the scenario  $S1$  is the one chosen by nature. For scenarios **S2** and **S3** there is a depletion around 1.2 TeV, and then the significance increases around 1.3 TeV, this can be explained by the slightly better performance of the BDT for the 1.3 TeV mass regarding 1.2 TeV.

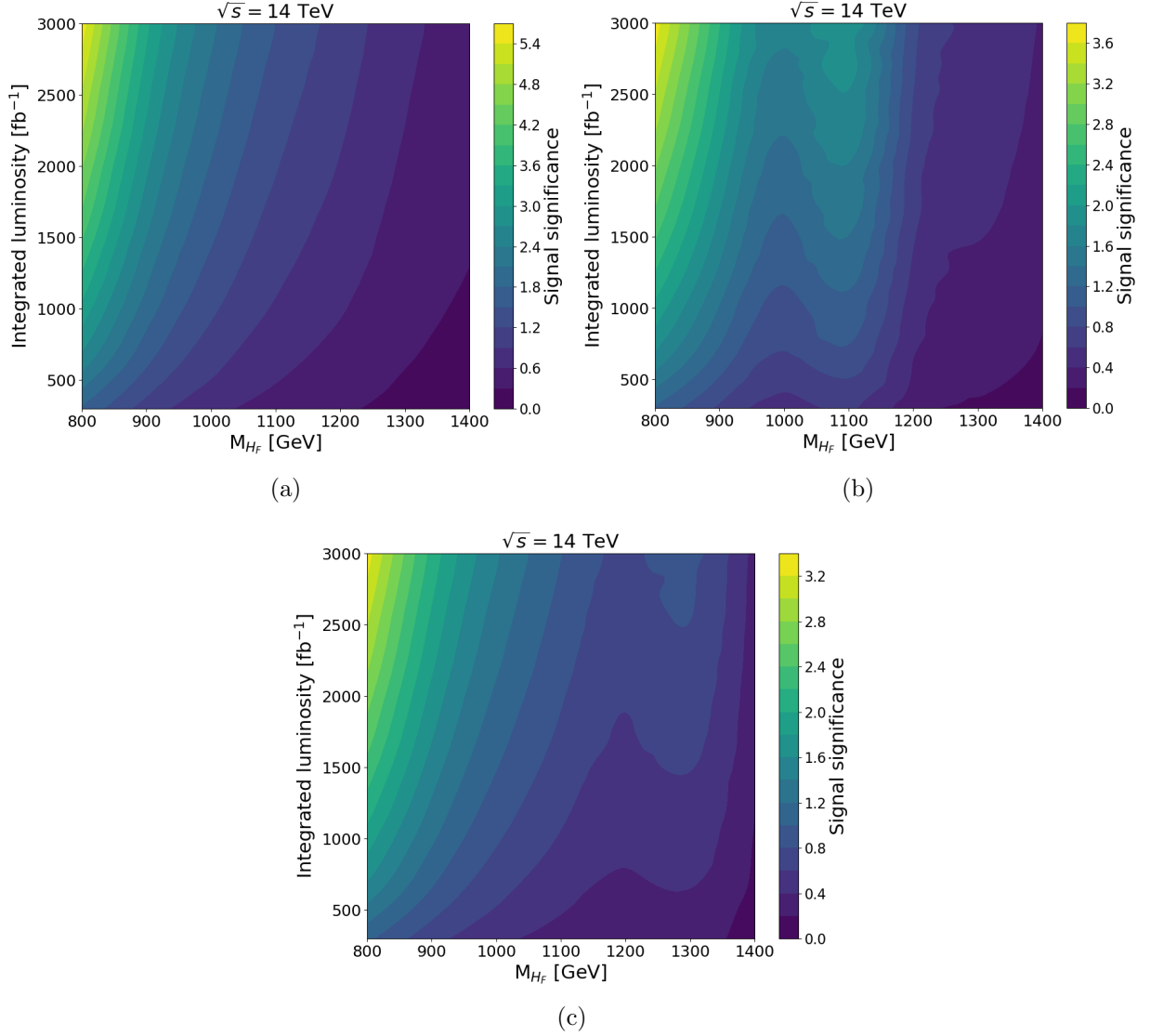


FIG. 11: Density plot showing the *signal significance* for the  $h \rightarrow b\bar{b}$  channel as a function of the integrated luminosity and the flavon mass  $M_{H_F}$ : (a) **S1**, (b) **S2** and (c) **S3**.

Meanwhile, Fig. 12 shows the *signal significance* as a function of luminosity and the flavon mass  $M_{H_F}$  for the  $pp \rightarrow H_F \rightarrow hb\bar{b}(h \rightarrow \gamma\gamma)$  process. In this channel, the sensitivity is lower than in the previous one because there is a factor of  $10^{-3}$  that suppresses the previous case, such a factor comes from the  $\mathcal{BR}(h \rightarrow \gamma\gamma) \sim 10^{-3}$ . However, considering that a future 100 TeV collider is a possibility [40], it is important to note that our calculations estimate that for a luminosity of  $30 \text{ ab}^{-1}$ , the sensitivity could reach up to  $5\sigma$ .

Finally, to highlight the usefulness of BDT, in Table VIII we present the *signal significance* for

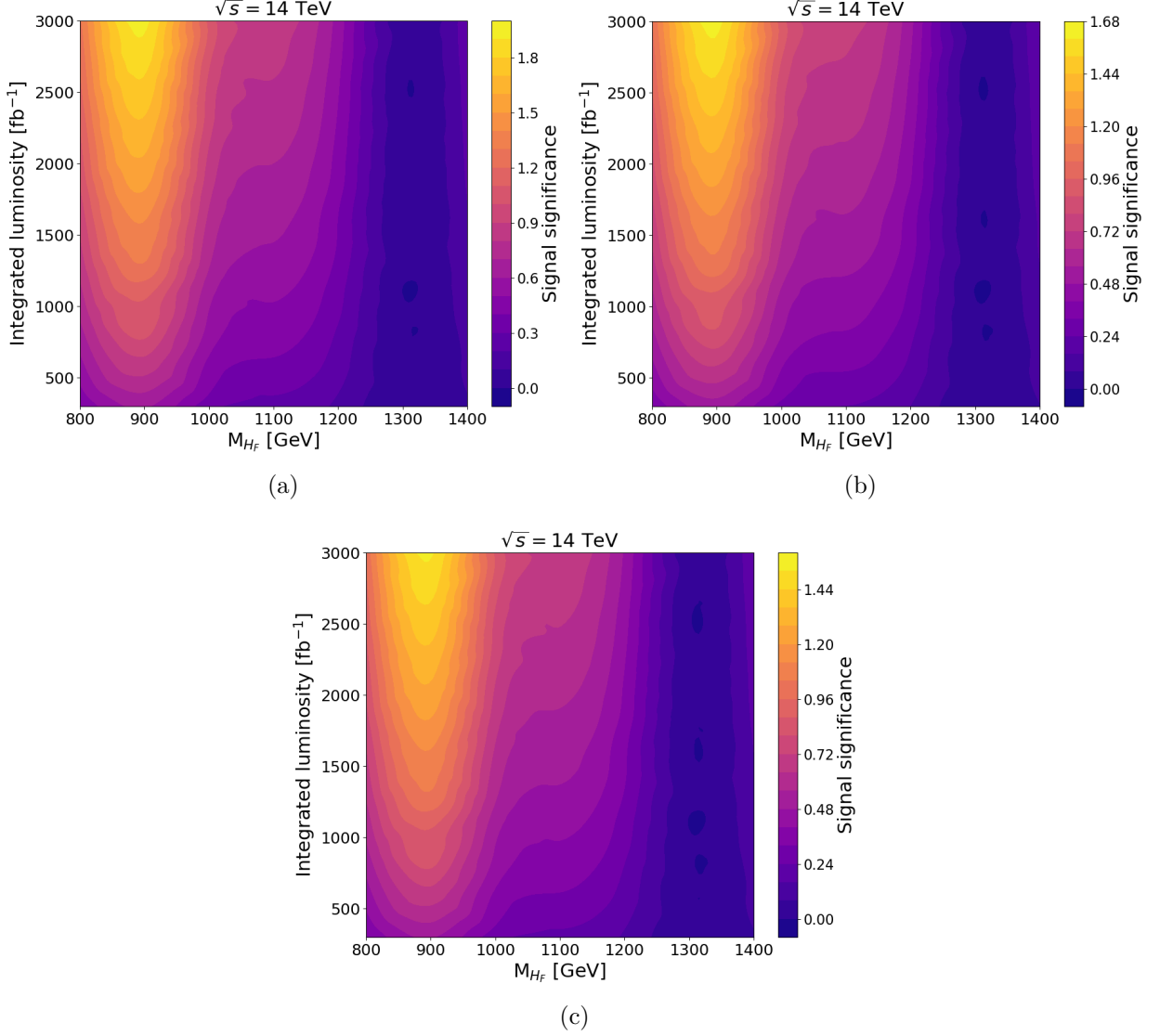


FIG. 12: Density plot showing the *signal significance* for the  $h \rightarrow \gamma\gamma$  channel as a function of the integrated luminosity and the flavon mass  $M_{H_F}$ : (a) **S1**, (b) **S2** and (c) **S3**.

the  $h \rightarrow b\bar{b}$  channel, where we have considered the basic cut, included in the HL-LHC card [41], and the following kinematic cuts for  $M_{H_F} = 800$  GeV:

1.  $p_T(b_{1,2,3,4}) > 80, 60, 50, 25$  GeV,
2.  $650 < M_{\text{inv}}(b_1 b_2 b_3 b_4) < 900$  GeV,
3. Combined transverse momentum  $p_T(b_1 b_2 b_3 b_4) > 550$  GeV.

Therefore, we conclude that the use of BDT substantially improves the isolation of the proposed signals.

TABLE VIII: Signal significance for the channel  $h \rightarrow b\bar{b}$  and  $\mathcal{L}_{\text{int}}=3000 \text{ fb}^{-1}$ .

$M_{H_F}$ (GeV)	Signal Significance
800	$1.75 \sigma$
900	$0.87\sigma$
1000	$0.4872\sigma$

## V. CONCLUSIONS

In this paper we studied the possibility of observing the  $pp \rightarrow H_F \rightarrow hb\bar{b}$  process through two channels in which the Higgs boson decays, namely,  $h \rightarrow b\bar{b}$  and  $h \rightarrow \gamma\gamma$ . The  $H_F$  mother particle is a predicted state in a model that extends the Standard Model and incorporates the Froggatt-Nielsen mechanism which is an opportunity to explain the mass hierarchy. Our predictions consider realistic scenarios for the free parameters of the model, which were extracted by analyzing theoretical and experimental constraints. We identify specific regions of the model parameter space in which we found *signal significances* of up to  $5\sigma$  ( $2\sigma$ ) for the  $h \rightarrow b\bar{b}$  ( $h \rightarrow \gamma\gamma$ ) channel. The study was based on the High Luminosity Large Hadron Collider which aims  $3000 \text{ fb}^{-1}$  of accumulated data at 14 TeV.

### Acknowledgments

The work of Marco A. Arroyo-Ureña and T. Valencia-Pérez is supported by “Estancias posdoctorales por México (SECIHTI)” and “Sistema Nacional de Investigadores” (SNII-SECIHTI). T.V.P. acknowledges support from the UNAM project PAPIIT IN11224 and the CONAHCYT project CBF2023-2024-548. E. A. Herrera-Chacón acknowledges support from CONAHCYT.

- 
- [1] **ATLAS** Collaboration, G. Aad et al., “Observation of a new particle in the search for the Standard Model Higgs boson with the ATLAS detector at the LHC,” [Phys. Lett. B \*\*716\*\* \(2012\) 1–29](#), [arXiv:1207.7214 \[hep-ex\]](#).
- [2] **CMS** Collaboration, S. Chatrchyan et al., “Observation of a New Boson at a Mass of 125 GeV with the CMS Experiment at the LHC,” [Phys. Lett. B \*\*716\*\* \(2012\) 30–61](#), [arXiv:1207.7235 \[hep-ex\]](#).
- [3] **ATLAS** Collaboration, G. Aad et al., “Search for nonresonant pair production of Higgs bosons in the  $b\bar{b}b\bar{b}$  final state in pp collisions at  $s=13 \text{ TeV}$  with the ATLAS detector,” [Phys. Rev. D \*\*108\*\* no. 5, \(2023\) 052003](#), [arXiv:2301.03212 \[hep-ex\]](#).
- [4] **ATLAS** Collaboration, G. Aad et al., “Search for pair production of boosted Higgs bosons via vector-boson fusion in the  $b\bar{b}b\bar{b}$  final state using  $pp$  collisions at  $\sqrt{s} = 13 \text{ TeV}$  with the ATLAS detector,” [arXiv:2404.17193 \[hep-ex\]](#).

- [5] **ATLAS** Collaboration, G. Aad *et al.*, “Studies of new Higgs boson interactions through nonresonant HH production in the  $b\bar{b}\gamma\gamma$  final state in pp collisions at  $\sqrt{s} = 13$  TeV with the ATLAS detector,” [JHEP \*\*01\*\* \(2024\) 066](#), [arXiv:2310.12301 \[hep-ex\]](#).
- [6] **ATLAS** Collaboration, G. Aad *et al.*, “Search for the non-resonant production of Higgs boson pairs via gluon fusion and vector-boson fusion in the  $b\bar{b}\tau^+\tau^-$  final state in proton-proton collisions at  $\sqrt{s} = 13$  TeV with the ATLAS detector,” [arXiv:2404.12660 \[hep-ex\]](#).
- [7] **ATLAS** Collaboration, G. Aad *et al.*, “Search for non-resonant Higgs boson pair production in the  $2b + 2\ell + E_T^{\text{miss}}$  final state in pp collisions at  $\sqrt{s} = 13$  TeV with the ATLAS detector,” [JHEP \*\*02\*\* \(2024\) 037](#), [arXiv:2310.11286 \[hep-ex\]](#).
- [8] C. D. Froggatt and H. B. Nielsen, “Hierarchy of Quark Masses, Cabibbo Angles and CP Violation,” [Nucl. Phys. B \*\*147\*\* \(1979\) 277–298](#).
- [9] M. Bauer, T. Schell, and T. Plehn, “Hunting the Flavon,” [Phys. Rev. D \*\*94\*\* no. 5, \(2016\) 056003](#), [arXiv:1603.06950 \[hep-ph\]](#).
- [10] E. Barradas-Guevara, J. L. Diaz-Cruz, O. Félix-Beltrán, and U. J. Saldana-Salazar, “Linking LFV Higgs decays  $h \rightarrow \ell_i\ell_j$  with CP violation in multi-scalar models,” [arXiv:1706.00054 \[hep-ph\]](#).
- [11] Arroyo-Ureña, Marco A. and Chakraborty, Amit and Díaz-Cruz, J. Lorenzo and Ghosh, Dilip Kumar and Khan, Najimuddin and Moretti, Stefano, “Flavon signatures at the HL-LHC,” [Phys. Rev. D \*\*108\*\* no. 9, \(2023\) 095026](#), [arXiv:2205.12641 \[hep-ph\]](#).
- [12] M. A. Arroyo-Ureña, J. L. Díaz-Cruz, G. Tavares-Velasco, A. Bolaños, and G. Hernández-Tomé, “Searching for lepton flavor violating flavon decays at hadron colliders,” [Phys. Rev. D \*\*98\*\* no. 1, \(2018\) 015008](#), [arXiv:1801.00839 \[hep-ph\]](#).
- [13] M. A. Arroyo-Ureña, A. Fernández-Télez, and G. Tavares-Velasco, “Flavor changing flavon decay  $\phi \rightarrow tc$  ( $\phi = H_F, A_F$ ) at the high luminosity large hadron collider,” [Rev. Mex. Fis. \*\*69\*\* no. 2, \(2023\) 020803](#), [arXiv:1906.07821 \[hep-ph\]](#).
- [14] N. Khan and S. Rakshit, “Study of electroweak vacuum metastability with a singlet scalar dark matter,” [Phys. Rev. D \*\*90\*\* no. 11, \(2014\) 113008](#), [arXiv:1407.6015 \[hep-ph\]](#).
- [15] G. Cynolter, E. Lendvai, and G. Pocsik, “Note on unitarity constraints in a model for a singlet scalar dark matter candidate,” [Acta Phys. Polon. B \*\*36\*\* \(2005\) 827–832](#), [arXiv:hep-ph/0410102](#).
- [16] **ATLAS** Collaboration, G. Aad *et al.*, “Search for Higgs boson pair production in the two bottom quarks plus two photons final state in  $pp$  collisions at  $\sqrt{s} = 13$  TeV with the ATLAS detector,” [Phys. Rev. D \*\*106\*\* no. 5, \(2022\) 052001](#), [arXiv:2112.11876 \[hep-ex\]](#).
- [17] **Particle Data Group** Collaboration, S. Navas *et al.*, “Review of particle physics,” [Phys. Rev. D \*\*110\*\* no. 3, \(2024\) 030001](#).
- [18] **CMS** Collaboration, A. M. Sirunyan *et al.*, “Search for lepton-flavor violating decays of the Higgs boson in the  $\mu\tau$  and  $e\tau$  final states in proton-proton collisions at  $\sqrt{s} = 13$  TeV,” [Phys. Rev. D \*\*104\*\* no. 3, \(2021\) 032013](#), [arXiv:2105.03007 \[hep-ex\]](#).
- [19] **ATLAS** Collaboration, G. Aad *et al.*, “Searches for lepton-flavour-violating decays of the Higgs boson into  $e\tau$  and  $\mu\tau$  in  $\sqrt{s} = 13$  TeV  $pp$  collisions with the ATLAS detector,” [JHEP \*\*07\*\* \(2023\)](#)



- 166, [arXiv:2302.05225 \[hep-ex\]](#).
- [20] M. A. Arroyo-Ureña, R. Gaitán, and T. A. Valencia-Pérez, “SpaceMath version 1.0 A Mathematica package for beyond the standard model parameter space searches,” [Rev. Mex. Fis. E](#) **19** no. 2, (2022) 020206, [arXiv:2008.00564 \[hep-ph\]](#).
- [21] A. J. Buras, F. D. Fazio, J. Girrbach, R. Kneijens, and M. Nagai, “The anatomy of neutral scalars with fncs in the flavour precision era,” [JHEP](#) **1306** (2013) 111, [arXiv:1303.3723 \[hep-ph\]](#).
- [22] A. Crivellin, A. Kokulu, and C. Greub, “Flavor-phenomenology of two-higgs-doublet models with generic yukawa structure,” [Phys. Rev. D](#) **87** no. 9, (2013) 094031, [arXiv:1303.5877 \[hep-ph\]](#).
- [23] M. Bona *et al.*, “Model-independent constraints on  $\delta f = 2$  operators and the scale of new physics,” [Journal of High Energy Physics](#) **2008** no. 03, (2008) 049.  
<http://www.utfit.org/UTfit/>. UTfit Collaboration.
- [24] **UTfit** Collaboration, A. J. Bevan *et al.*, “The utfit collaboration average of d meson mixing data: Winter 2014,” [JHEP](#) **1403** (2014) 123, [arXiv:1402.1664 \[hep-ph\]](#).
- [25] G. Abbas, A. K. Alok, N. R. S. Chundawat, N. Khan, and N. Singh, “Finding flavons at colliders,” [Phys. Rev. D](#) **110** no. 11, (2024) 115015, [arXiv:2407.09255 \[hep-ph\]](#).
- [26] T. Plehn, “Lectures on LHC Physics,” [Lect. Notes Phys.](#) **844** (2012) 1–193, [arXiv:0910.4182 \[hep-ph\]](#).
- [27] A. Pak, M. Rogal, and M. Steinhauser, “Production of scalar and pseudo-scalar Higgs bosons to next-to-next-to-leading order at hadron colliders,” [JHEP](#) **09** (2011) 088, [arXiv:1107.3391 \[hep-ph\]](#).
- [28] **LHC Higgs Cross Section Working Group** Collaboration, D. de Florian *et al.*, “Handbook of LHC Higgs Cross Sections: 4. Deciphering the Nature of the Higgs Sector,” [arXiv:1610.07922 \[hep-ph\]](#).
- [29] A. Alloul, N. D. Christensen, C. Degrande, C. Duhr, and B. Fuks, “FeynRules 2.0 - A complete toolbox for tree-level phenomenology,” [Comput. Phys. Commun.](#) **185** (2014) 2250–2300, [arXiv:1310.1921 \[hep-ph\]](#).
- [30] J. Alwall, R. Frederix, S. Frixione, V. Hirschi, F. Maltoni, O. Mattelaer, H. S. Shao, T. Stelzer, P. Torrielli, and M. Zaro, “The automated computation of tree-level and next-to-leading order differential cross sections, and their matching to parton shower simulations,” [JHEP](#) **07** (2014) 079, [arXiv:1405.0301 \[hep-ph\]](#).
- [31] T. Sjöstrand, S. Ask, J. R. Christiansen, R. Corke, N. Desai, P. Ilten, S. Mrenna, S. Prestel, C. O. Rasmussen, and P. Z. Skands, “An introduction to PYTHIA 8.2” [Comput. Phys. Commun.](#) **191** (2015) 159–177, [arXiv:1410.3012 \[hep-ph\]](#).
- [32] **DELPHES 3** Collaboration, J. de Favereau, C. Delaere, P. Demin, A. Giammanco, V. Lemaître, A. Mertens, and M. Selvaggi, “DELPHES 3, A modular framework for fast simulation of a generic collider experiment,” [JHEP](#) **02** (2014) 057, [arXiv:1307.6346 \[hep-ex\]](#).
- [33] M. Cacciari, G. P. Salam, and G. Soyez, “FastJet User Manual,” [Eur. Phys. J. C](#) **72** (2012) 1896, [arXiv:1111.6097 \[hep-ph\]](#).

- [34] E. Conte, B. Fuks, and G. Serret, “MadAnalysis 5, A User-Friendly Framework for Collider Phenomenology,” [Comput. Phys. Commun.](#) **184** (2013) 222–256, [arXiv:1206.1599 \[hep-ph\]](#).
- [35] M. Cacciari, G. P. Salam, and G. Soyez, “The anti- $k_t$  jet clustering algorithm,” [JHEP](#) **04** (2008) 063, [arXiv:0802.1189 \[hep-ph\]](#).
- [36] **ATLAS** Collaboration, G. Aad et al., “Fast b-tagging at the high-level trigger of the ATLAS experiment in LHC Run 3,” [JINST](#) **18** no. 11, (2023) P11006, [arXiv:2306.09738 \[hep-ex\]](#).
- [37] L. Breiman et al., [Classification and regression trees](#). Wadsworth international group, California, USA, 1984.
- [38] T. Chen and C. Guestrin, “XGBoost: A scalable tree boosting system,” in [Proc. 22nd ACM SIGKDD Int. Conf. on Knowledge Discovery and Data Mining, KDD '16](#), p. 785. ACM, New York, NY, USA, 2016.
- [39] J. Bergstra, D. Yamins, and D. Cox, “Making a science of model search: Hyperparameter optimization in hundreds of dimensions for vision architectures,” in [Proceedings of the 30th International Conference on Machine Learning](#), S. Dasgupta and D. McAllester, eds., vol. 28 of [Proceedings of Machine Learning Research](#), pp. 115–123. PMLR, Atlanta, Georgia, USA, 17–19 jun, 2013. <https://proceedings.mlr.press/v28/bergstra13.html>.
- [40] N. Arkani-Hamed, T. Han, M. Mangano, and L.-T. Wang, “Physics opportunities of a 100 tev proton–proton collider,” [Physics Reports](#) **652** (2016) 1–49. <https://www.sciencedirect.com/science/article/pii/S0370157316301855>. Physics opportunities of a 100 TeV proton–proton collider.
- [41] M. Selvaggi, “Beta card for HL-LHC and HE-LHC studies.” 2017. [https://github.com/delphes/delphes/blob/master/cards/delphes\\_card\\_HLLHC.tcl](https://github.com/delphes/delphes/blob/master/cards/delphes_card_HLLHC.tcl).